Plant Physiology and Biochemistry 144 (2019) 300–311

Contents lists available at ScienceDirect

Plant Physiology and Biochemistry

journal homepage: www.elsevier.com/locate/plaphy

Research article

Performance of optimized hyperspectral reflectance indices and partial least squares regression for estimating the chlorophyll fluorescence and grain yield of wheat grown in simulated saline field conditions

Salah El-Hendawy[a,b,*], Nasser Al-Suhaibani[a], Salah Elsayed[c], Majed Alotaibi[a], Wael Hassan[d,e], Urs Schmidhalter[f]

[a] Department of Plant Production, College of Food and Agriculture Sciences, King Saud University, P.O. Box 2460, 11451, Riyadh, Saudi Arabia
[b] Department of Agronomy, Faculty of Agriculture, Suez Canal University, Ismailia, 41522, Egypt
[c] Evaluation of Natural Resources Department, Environmental Studies and Research Institute, University of Sadat City, Menoufia, 32897, Egypt
[d] Department of Agricultural Botany, Faculty of Agriculture, Suez Canal University, Ismailia, 41522, Egypt
[e] Department of Biology, College of Science and Humanities at Quwayiah, Shaqra University, Riyadh, 11961, Saudi Arabia
[f] Department of Plant Science, Chair of Plant Nutrition, Technical University of Munich, Freising, Germany

ARTICLE INFO

Keywords:
Non-photochemical quenching
Phenotyping
Physiology
Quantum yield of PSII
Salinity stress
Subsurface water retention technique

ABSTRACT

To overcome the salinity threats to crop production in arid conditions, wheat cultivars should be developed with better performance with regard to key physiological traits. Although different chlorophyll fluorescence (ChlF) parameters, such as maximum quantum PSII photochemical efficiency (*Fv/Fm*), quantum yield of PSII (Φ_{PSII}), and non-photochemical quenching (NPQ) have been proven to be key physiological traits to improve salt tolerance, their evaluation is time-consuming. In this study, hyperspectral canopy reflectance was used to assess ChlF parameters and grain yield (GY) of two wheat cultivars growing in simulated saline field conditions and exposed to three salinity levels (control, 6.0 dS m^{-1}, and 12.0 dS m^{-1}). Different spectral reflectance indices (SRIs) were formulated as ratios based on contour maps and tested for their relationship with ChlF parameters. The performance of individual SRIs and partial least squares regression (PLSR) models based on ChlF parameters, all examined SRIs, or data fusion of combined ChlF and SRIs to estimate the GY was considered. All examined SRIs failed to assess Φ_{PSII} and NPQ under control condition, but most of them showed a moderate to strong relationship with both parameters under the salinity levels of 6.0 and 12.0 dS m^{-1}. The examined SRIs showed a moderate and strong relationship with *Fv/Fm* under conditions of 6.0 and 12.0 dS m^{-1}, respectively. Most SRIs correlated better with the three ChlF parameters for the salt-sensitive cultivar Sakha 61 than for the salt-tolerant cultivar Sakha 93. Several SRIs exhibited strong relationships with GY under the salinity levels of 6.0 and 12.0 dS m^{-1} and for both cultivars. Overall, the PLSR models exhibited additional improvements for estimating and predicting GY in both calibration and validation datasets over that using individual SRIs. The PLSR model based on data fusion was the best model to accurately estimate GY in the validation model even under control conditions. This study, of a type rarely conducted in simulated saline field conditions, indicates that the ChlF parameters could be linked to hyperspectral reflectance data for the rapid and non-destructive assessment of photosynthetic status and prediction of wheat production under salt stress field conditions.

1. Introduction

Salinity stress limits growth and productivity of plants through its negative effects on several fundamental physiological and biochemical properties. These properties can be inhibited by different components of salinity stress, such as osmotic and ion toxicity stresses, as well as a deficit of essential ions, especially K^+, Mg^{2+}, and Ca^{2+} (Zhang et al., 2014; El-Hendawy et al., 2017a). The different components of salinity stress interact together to inhibit or cause disorder in the process related to photosynthetic capacity of plants, eventually leading to a severe reduction in plant productivity (Chen and Murata, 2011; Zhang et al., 2011). Low osmotic potential of the soil solution due to high salt

* Corresponding author. Department of Plant Production, College of Food and Agriculture Sciences, King Saud University, P.O. Box 2460, 11451, Riyadh, Saudi Arabia.
E-mail addresses: mosalah@ksu.edu.sa, shendawy@yahoo.com, shendawy2003@gmail.com (S. El-Hendawy).

https://doi.org/10.1016/j.plaphy.2019.10.006
Received 3 June 2019; Received in revised form 3 October 2019; Accepted 3 October 2019
Available online 04 October 2019
0981-9428/

concentrations results in a significant decrease in leaf water potential, subsequently leading to partial stomatal closure and ultimately to decreased photosynthesis efficiency (Najafi et al., 2007; Ahmed et al., 2013). The excessive build-up of toxic ions (Na^+ and Cl^-) in the leaves or an imbalance of ionic concentrations between Na^+ and other essential ions leads to detrimental effects on plant photosynthetic system by inducing damage to the operating efficiency of photosystem II (PSII) and chlorophyll ultrastructure (Baker and Rosenqvist, 2004; Chen and Murata, 2011). The damage to PSII is directly accompanied by disturbances in the chlorophyll fluorescence (ChlF) and CO_2 assimilation (Naumann et al., 2008a). Therefore, there is no doubt that assessment of different ChlF parameters can provide valuable information about the status of plant photosynthetic performance under salinity stress conditions (Baker and Rosenqvist, 2004; Zhang et al., 2011).

Several studies have reported that salinity stress causes a significant decline in the maximum quantum PSII photochemical efficiency (*Fv/Fm*) and the quantum yield of PSII (Φ_{PSII}), whereas leading to increases the non-photochemical quenching (NPQ) (Baker, 2008; El-Hendawy et al., 2017a). Therefore, the parameters of ChlF, which are indicators of photosynthetic functions, can be used as evaluation criteria for salt tolerance (Abdeshahian et al., 2010; Zhang et al., 2012; El-Hendawy et al., 2017a; Peng et al., 2017).

ChlF is emitted by chlorophyll in the red and far-red light (600–800 nm) spectra with two distinct peaks located between 685-690 nm and 730–740 nm but with a maximum peak at 690 and 740 nm, respectively (Lichtenthaler and Miehé, 1997; Buschmann et al., 2000). However, the positions of these emission bands are sometimes affected by re-absorption of the red part of the spectrum because this part overlaps with the absorption of the spectrum by chlorophyll (Gitelson et al., 1998). Although the ChlF of plants emit only 2–5% of the absorbed light energy, this emitted light carries valuable information about several biochemical and physiological status, which respond to the onset of different abiotic stress before irreversible morphological damages are visible (Zarco-Tejada et al., 2003; Zhang et al., 2012; Kalariya et al., 2019).

The measurement of ChlF by traditional methods using a portable fluorimeter is time-consuming, and it is difficult to track their changes frequently for a large-scale area and large numbers of genotypes. Importantly, although the ChlF can be detected in a non-destructive manner using fluorometers, this device traces the changes in ChlF based on only effective one or two leaves with disregarding the vertical variability in ChlF that is associated with distinct variation in age and position of leaves within the plant canopy (Jin et al., 2004). Therefore, a more efficient tool is needed to track the changes in ChlF at the whole canopy level. ChlF emissions can be detected using either a based ground-mounted sensor, aerial imaging, or space-borne sensors at the canopy level (Porcar-Castell et al., 2014; Peng et al., 2017).

A based ground-mounted sensor which is able to detect the spectral reflectance of a canopy in the range of visible (VIS) to shortwave infrared (SWIR) is one of the efficient tools used for tracking changes that take place in different biochemical and biophysical properties of the leaves in a quick and non-destructive manner. (Mariotto et al., 2013; Rapaport et al., 2017; El-Hendawy et al., 2019a). The spectral reflectance from the canopy in the range of 350–2500 nm can be exploited to derive specific spectral reflectance indices (SRIs). Several studies have exploited the SRIs that indicate changes in chlorophyll content, photosynthetic activity, leaf area index, and leaf water content to indirectly estimate ChlF under different nitrogen treatments or water stress levels (Jia et al., 2016; Peng et al., 2017; Rapaport et al., 2017; Kováč et al., 2018; Sancho-Knapik et al., 2018). For example, Peng et al. (2017) found that SRIs that included wavelengths from the long-wave red edge and NIR, such as the normalized difference red edge index ($NDRE_{740}$), the red edge chlorophyll index (CI_{740}), as well as the wavelengths in the spectral range of 700–900 nm are well correlated with Fv/Fm under irrigated and water stress conditions. Jia et al. (2016) also reported that the red edge position at leaf level is highly related to *Fv/Fm* of wheat under different nitrogen levels. Rapaport et al. (2017) found that water balance index (WABI), which formulated from one wavelength from the VIS region (c. 531 nm) and one from the SWIR (c. 1500 nm), could be used to monitor NPQ of grapevine, pea, and sunflower under different irrigation conditions; the physiological reflectance index (PRI) and structure intensive pigment index (SIPI) varied similarly and had a strong relationship with different ChlF parameters like NPQ and Φ_{PSII} (Miloš et al., 2018; Sancho-Knapik et al., 2018).

It has been reported that most of the conventional chlorophyll-related SRIs are not always efficient to track the changes in ChlF under stress conditions, with the exception of the PRI, which has been linked to the rapid changes in xanthophyll cycle induced by different types of stress (Gamon et al., 1992; Naumann et al., 2008a). In addition, it is also observed that the content of photosynthetic pigment is not directly associated with quick changes in photosynthetic processes and cannot explain the down regulation of photosynthesis due to early environmental stresses (Anser and Alencar, 2010; Zhang et al., 2014). Therefore, the published SRIs linked to chlorophyll contents need to be modified or new ones have to be reported to assess the ChlF under environmental abiotic stress, such as salinity stress.

Dobrowski et al. (2005) reported that the SRIs that utilize the wavelengths located out of the absorption regions for chlorophyll and carotenoid pigments, such as R_{690}/R_{600} and R_{740}/R_{800}, tracked the changes in ChlF more effectively than the conventional chlorophyll-related SRIs, due to potentially minimizing the influence of different chlorophyll pigment concentrations on the signal of Chlf through re-absorption. At the canopy level, the simple spectral reflectance ratio index or normalized index constructed from the sensitive hyperspectral wavelengths of 680 and 935 nm were found to be effective for assessing responses of different ChlF parameters to salt stress (Zhang et al., 2012). The simple ratio index (R_{690}/R_{630}) has been found to be more effective for the assessment of *Fv/Fm* under drought stress than the PRI due to the relation with ChlF emission and not with chlorophyll pigments (Zhang et al., 2017). Some studies have also reported that reflectance ratios indices combining the red, red edge, and NIR wavelength such as R_{690}/R_{630}, R_{690}/R_{655}, R_{690}/R_{740}, and R_{730}/R_{706} were sensitive to changes of ChlF, because the ChlF signal is superimposed on the red-edge of leaf reflectance (Lichtenthaler and Miehé, 1997; Meroni et al., 2009; Zhang et al., 2017). Since the spectral reflectance patterns of the canopy have been found to be affected by several factors, there is a need to test the usefulness of published SRIs when they are applied to different environmental conditions, abiotic stress, and crops or when used for the assessment of other plant parameters, as some SRIs may be more suitable for certain conditions but could not be applied to other conditions (Filella et al., 2004; Naumann et al., 2008a; El-Hendawy et al., 2019b).

Plant breeders often consider the final grain yield, per se, as fundamental screening criteria for evaluating the salt tolerance of genotypes. However, due to a high genotype-environment interaction and low heritability of this trait, plant breeders always looking for other effective screening criteria that show high heritability and strong correlation with grain yield (Babar et al., 2006). In addition, plant breeders exploit the close and true associations of morphological, physiological, and biochemical traits with grain yield to indirectly predict the final grain yield at the early stages of growth. Therefore, the different ChlF parameters can be used as indirect traits to predict of grain yield early and as an indicator to avoid loss of grain yield under salinity stress conditions (Zhang et al., 2011).

Instead of formulating SRIs, a whole range of spectrum is used as an empirical basis to prepare the best model in predicting the traits of interest. Partial least squares regression (PLSR) is a typical method that specifies a linear relationship between a set of independent and response variables and has been widely used (Sharabian et al., 2014; Garriga et al., 2017), since the measured traits can be simultaneously assessed through a wide range of wavelengths or SRIs from the VIS,

NIR, and SWIR of the spectrum regions. PLSR is a regression method that can be used to reduce a large number of measured collinear spectral factors to a few non-correlated latent factors. Thus, an optimal latent factor demonstrating calibration data without over-fitting could be used to predict the measured traits (Atzberger et al., 2010). PLSR as opposed to multiple linear regressions (MLR) allows removing correlated information, due to the fact that large numbers of wavebands in the selected waveband range from 350 to 2500 nm can be correlated to each other, thus avoiding redundant information. Previous studies have demonstrated the performance of PLSR methods for estimating different measured traits, such as biomass, leaf area index, grain yield, and water and nitrogen status of different crops (Li et al., 2014; Rischbeck et al., 2016; Feng et al., 2018).

Elsayed et al. (2017) found that the combination of SRIs that depends on the bands in the spectral range of 302–1148 with canopy temperature and water relations traits in a PLSR model, improved the prediction grain yield of wheat under both well-irrigated and water-deficit conditions. Because the information of spectral data collected from a canopy by passive or active reflectance sensors is limited to the interactions of spectra light with plants or soil material, employing information from different sensors based on other physical principles could add information to spectral measurements in order to assess the target yields. Therefore, statistical data fusion of sensor measurements (passive reflectance sensor and portable fluorimeter) coupled with PLSR models could improve the predictive power to assess the final grain yield under salinity stress conditions.

One inherent characteristic of natural saline field conditions is their spatial patchiness, with the salt concentrations in these patches ranging from low salt concentration to several folds higher than the concentration of salt in seawater (Bazihizina et al., 2012). For example, in irrigated fields, the horizontal variation in the salinity of the soil solution ranged from 0 to 24 dS m^{-1} over distances less than 10 m. The vertical variations in the salinity of the soil solution ranged from 4 to 20 dS m^{-1} over distances less than 1 m (Cetin and Kirda, 2003; Çullu et al., 2009). The inherent variability in soil salinity considerably affects the uniformity of individual plants' growth within the population even over short distances, especially for glycophytic plants such as wheat. Therefore, it is anticipated that it is difficult and inefficient to assess morpho-physiological traits and spectral reflectance patterns of wheat crops under heterogeneous soil salinity conditions. Because wheat reacts very sensitive to heterogeneous soil salinity conditions and to obtain a uniform plant growth of the plant population, saline field conditions in this study were simulated using a new method which called a subsurface water retention technique (SWRT). The advantages of this technique has been described in detail by El-Hendawy et al. (2017a,b) and El-Hendawy et al. (2019a,b).

The main objective of this study was to examine the suitability of different published and new SRIs for estimating different ChlF parameters (*Fv/Fm, Φ_{PSII} and NPQ*) and additionally to assess the final grain yield under different conditions (salinity levels, cultivars, and seasons). Since the final grain yield represents the main target for plant breeders as fundamental screening criterion for evaluating the salt tolerance of genotypes, and given that measurements of this trait remain expensive, laborious, and time-consuming, particularly when a large number of genotypes is evaluated, as well as that the SRIs focus mostly on few principle wavelengths which could result in SRIs that tend to be less efficient and inconsistent for assessing grain yield across different growing conditions, we tested one further objective as well to exhibit additional improvements for estimating GY. Therefore, the second objective of this study was to evaluate the ability of different PLSR models based on either three ChlF parameters, all examined SRIs, or the data fusion of both ChlF parameters and SRIs to predict the final grain yield of wheat cultivars under different conditions. By testing the two objectives of this study, we could compare the performance of individual SRIs and different models of PLSR in estimating the final grain yield under different conditions. In addition, we propose that fusing data for combining relevant non-spectral data (based on the leaf level) and spectral bands (based on the canopy level) could provide some additional improvements in the more accurate estimation of grain yield of wheat under different conditions.

2. Materials and methods

2.1. Plant materials and field experiment description

Two spring wheat cultivars, one salt-tolerant (Sakha 93) and the other salt-sensitive (Sakha 61), were grown under simulated saline field conditions using subsurface water retention technique (SWRT). This technique has been described in detail by El-Hendawy et al. (2017a,b) and El-Hendawy et al. (2019a,b). The main objective of using this technique was to overcome the temporal and spatial variations that take place in salt concentration and water content in the root zone, which are common in saline-affected soil in natural environment. In addition, this technique utilizes a representative sample size, a large measuring area for canopy hyperspectral reflectance measurement, and exposes all tested genotypes to fluctuations in parameters (humidity and temperature) that control the rate of evapotranspiration. An example for install this technique has been explained in detail in our previous study (El-Hendawy et al., 2017b).

The experiment was conducted at the Experimental Research Station of the College of Food and Agriculture Sciences, King Saud University, Riyadh, Saudi Arabia (24°25′N, 46°34′E; elevation 400 m). Rainfall and temperature conditions were 8–25 mm and 12.9–32.2 °C, respectively. The experimental soil texture was sandy (90.4% sand, 5.4% silt, and 4.2% clay), with a soil bulk density of about 1.48 g cm^{-3}, a field capacity of 0.101 m^3 m^{-3}, and a wilting point of 0.038 m^3 m^{-3} according to El-Hendawy et al. (2019b).

The experiment was conducted in a randomized complete block split-plot design with three replicates; the three salinity levels (control (0.35 dS m^{-1}), moderate salinity level (6.0 dS m^{-1}), and high salinity level (12.0 dS m^{-1})) and the two cultivars were assigned as the main plots and subplots, respectively. The wheat cultivars were sown in a four-row plot of a plot size 6 m × 0.6 m at a seeding rate of 15 g m^{-2}.

All the plots were first irrigated with fresh water for 24 d in order to avoid osmotic shock during germination and at the early seedling stage. Thereafter, the two salinity treatments (6.0 and 12.0 dS m^{-1}) were irrigated with artificial saline water containing 3.51 and 7.02 g NaCl L^{-1}, respectively. In order to monitor the build-up of salt concentrations in the root zone during the application of artificial saline water, soil samples at depths of 0–40 cm were collected from each sub plot before irrigation. The electrical conductivity (EC) of collected samples was measured using the soil water extract method, with the sample suspensions comprising a 2:1 water-to-soil ratio. To deliver equal and constant amounts of water to each sub plot, the main irrigation line, which delivered water from water storage tanks to each sub plot, was distributed to sub-main hoses in each sub plot and equipped with manual control valves.

The plants were fertilized with 180, 90, and 60 kg ha^{-1} of N, P_2O_5, and K_2O, respectively. The phosphorus and potassium fertilizers were applied prior to the sowing and at booting stages, respectively, whereas the nitrogen fertilizer was applied in three equal doses at the seeding, stem-elongation, and booting stages.

2.2. Chlorophyll fluorescence parameters and grain yield measurements

Chlorophyll fluorescence parameters (ChlF) were measured at the flowering stage in the youngest, fully expanded, and sun-exposed leaves of the three randomly selected plants from each plot using a portable fluorometer (PAM 2500, Walz, Effeltrich, Germany). If the reading of ChlF for the three representative plants differs by more than 10%, then a further reading were taken for the same plot. The mean value of each ChlF parameter for each cultivar was finally calculated as an average

Table 1
Algorithms corresponding to the spectral reflectance indices (SRIs) used in this study.

SRIs	Formula	References
Ratio of reflectance between 570 and 870 nm	R_{570}/R_{870}	This work
Ratio of reflectance between 630 and 550 nm	R_{630}/R_{550}	This work
Ratio of reflectance between 630 and 800 nm	R_{630}/R_{800}	This work
Ratio of reflectance between 630 and 1100 nm	R_{630}/R_{1100}	This work
Ratio of reflectance between 670 and 780 nm	R_{670}/R_{780}	This work
Ratio of reflectance between 780 and 531 nm	R_{780}/R_{531}	This work
Ratio of reflectance between 780 and 690 nm	R_{780}/R_{690}	This work
Ratio of reflectance between 970 and 690 nm	R_{970}/R_{690}	This work
Ratio of reflectance between 1100 and 670 nm	R_{1100}/R_{670}	This work
Ratio of reflectance between 1250 and 690 nm	R_{1250}/R_{690}	This work
Ratio of reflectance between 1650 and 531 nm	R_{1650}/R_{531}	This work
Ratio of reflectance between 1450 and 670 nm	R_{1450}/R_{670}	This work
Ratio of reflectance between 1950 and 750 nm	R_{1950}/R_{750}	This work
Ratio of reflectance between 1950 and 1050 nm	R_{1950}/R_{1050}	This work
Ratio of reflectance between 2250 and 670 nm	R_{2250}/R_{670}	This work
Normalized difference vegetation index (NDVI)	$(R_{800} - R_{670})/(R_{800} + R_{670})$	Tucker (1979)
Structural insensitive pigment index (SIPI)	$(R_{800} - R_{445})/(R_{800} + R_{680})$	Peñuelas et al. (1995)
Ratio of reflectance between 690 and 630 nm	R_{690}/R_{630}	Zhang et al. (2017)
Photochemical reflectance index (PR1)	$(R_{531} - R_{570})/(R_{531} + R_{570})$	Gamon et al. (1992)
Water balance index (WABI)	$(R_{1500} - R_{531})/(R_{1500} + R_{531})$	Rapaport et al. (2017)
Development water balance index (DWABI-1)	$(R_{1550} - R_{482})/(R_{1550} + R_{482})$	El-Hendawy et al. (2019b)
Development water balance index (DWABI-2)	$(R_{1640} - R_{482})/(R_{1640} + R_{482})$	El-Hendawy et al. (2019b)
Development water balance index (DWABI-3)	$(R_{1650} - R_{531})/(R_{1650} + R_{531})$	El-Hendawy et al. (2019b)
Development normalized difference moisture index (DNDMI)	$(R_{1660} - R_{1742})/(R_{1660} + R_{1742})$	El-Hendawy et al. (2019b)
Development dry matter content index (DDMCI)	$(R_{2305} - R_{1550})/(R_{2305} + R_{1550})$	El-Hendawy et al. (2019b)
Red edge chlorophyll index ($CI1_{705}$)	$(R_{780}/R_{705}) - 1$	Gitelson et al. (2003)
Red edge chlorophyll index (CI_{740})	$(R_{780}/R_{740}) - 1$	Gitelson et al. (2005)
Green chlorophyll index (CI_{green})	$(R_{780}/R_{560}) - 1$	Gitelson et al. (2003)
Normalized difference red edge index ($NDRE_{740}$)	$(R_{780} - R_{740})/(R_{780} + R_{740})$	Gitelson and Merzlyak (1997)
The MERIS terrestrial chlorophyll index (MTCI)	$(R_{780} - R_{705})/(R_{705} + R_{665})$	Dash and Curran (2004)

measurement of three replications and three plants. The minimal chlorophyll fluorescence (*Fo*) was measured on the dark-adapted leaves using modulated light ($< 0.1\ \mu mol\ m^{-2}\ s^{-1}$), while the maximal chlorophyll fluorescence in the dark (*F*m) was measured using a 0.8 s pulse of $8000\ \mu mol\ m^{-2}\ s^{-1}$ of white light. Subsequently, the same dark-adapted leaves were exposed to actinic light ($5000\ \mu mol\ m^{-2}\ s^{-1}$) until the chlorophyll fluorescence at steady-state photosynthesis (*Fs*) was reached and recorded, and a second pulse of high-intensity white light ($8000\ \mu mol\ m^{-2}\ s^{-1}$) was applied to determine the maximal chlorophyll fluorescence (F'_m) in the light-adapted state. Leaves were then covered with a dark cloth and the minimal fluorescence (F'_o) after applying far-red light ($7\ \mu mol\ m^{-2}\ s^{-1}$) was recorded. The variable fluorescence (F_v) was calculated from the measurements of F_o and F_m values as $F_m - F_o$. The maximum quantum PSII photochemical efficiency was calculated as F_v/F_m. The actual PSII efficiency (Φ_{PSII}) and non-photochemical quenching (NPQ) were calculated as $(F'_m - F_s)/F'_m$) and $(F_m - F'_m)/F'_m$), respectively.

When plants reached maturity, 50 plants from each subplot were randomly selected to determine the weight of grains per plant. The grain yield (GY) was determined after the moisture content in the grains was adjusted to approximately 14%.

2.3. Hyperspectral reflectance measurements

Along with measurement of ChlF, canopy hyperspectral reflectance was measured using a portable backpack ASD spectroradiometer (Analytical Spectral Devices Inc., Boulder, CO, USA), which captured the reflectance from the canopy from 350 to 2500 nm using an optical fiber probe with a 25° field of view. The sampling intervals of the spectra were 1.4 and 2.2 nm, ranging from 350 to 1000 nm and 1000–2500 nm, respectively, whereas the full spectrum range (350–2500 nm) was finally calculated automatically to resample at continuous bands of 1.0-nm. The canopy reflectance was collected within ± 2 h of solar noon under cloudless conditions. The optical fiber probe was held vertically at approximately 0.80 m above the canopy in the nadir orientation to sense an area of 23.4 cm in diameter. A Spectralon reflectance panel (Labsphere, Inc., North Sutton, NH, USA) was used to calibrate the spectroradiometer before measurements and when needed during the measurements. Five replicated (five shots) hyperspectral measurements, each representing an average of 10 scans, were taken for each plot at different places on the central of second and third row. Finally, the average of five measurements was recorded as the measured spectrum for a plot.

2.4. Newly developed spectral reflectance indices and selection of published indices from literature

Contour maps of relevant statistical parameters, such as coefficients of determination (R^2) between the ChlF parameters, and grain yield and spectral indices were calculated from combinations of two individual bands from 350 to 2500 nm. The R package “lattice” from the software R statistics version 3.0.2 (R foundation for statistical computing 2013, Vienna, Austria) was used to draw the contour maps for spectral reflectance data. The newly developed SRIs in this study were selected based on hotspots of higher R^2 values in the contour maps, which represent all possible dual wavelengths combinations from binary, efficient extraction of significant peak-wavelengths, and the extent of effective regions which are related to the relationships between apparent reflectance and the measured parameters. Interestingly, the new SRIs were based on combined information from the photosynthetic pigment and fluorescence emission bands, and photosynthetic activity (determined by xanthophyll pigments) in the visible (VIS, 531, 550, 570, 630, 670, and 690 nm) and red edge (750 and 780 nm) regions, weak absorption bands located in the near-infrared (NIR, 800, 870, 970, 1050, 1100, and 1250 nm) region, and the strong water absorption bands found in the shortwave-infrared (SWIR, 1450, 1650, 1950, and 2250 nm) region. The newly developed and fifteen published SRIs are listed with references in Table 1.

2.5. Statistical analysis

The relationships between the ChlF parameters and GY, as well as the relationship between SRIs and measured parameters were tested using regressions analysis. The significance levels for R^2 were determined at 0.05 probability level. Different statistical parameters were used to evaluate the fit of the different models of PLSR between the predicted and observed values. These statistical parameters included the coefficient of determination (R^2), the root mean square error (RMSE), and the intercept and slope of the linear regression between the observed and predicted values for each measured parameter.

The multivariate data analysis software, Unscrambler 10.2 (CAMO Software AS, Oslo), was used to calibrate and validate PLSR models. After the spectrum was obtained, PLSR was implemented to obtain information concerning the measured parameters. The calibration models derived from two seasons dataset of PLSR models based on the three ChlF parameters (F_v/F_m, Φ_{PSII}, and NPQ), 30 SRIs presented in Table 1, and the data fusion of both ChlF parameters and SRIs were utilized to predict the final GY of wheat cultivars under different conditions (salinity levels, cultivars, and seasons). The different models of PLSR were calibrated using the dataset of pooled data through cross-validation, and subsequently the equations of calibration of different models (Table 5) were used to predict the GY (as independent data) for each salinity level, cultivar, and season. The x indicated in Tables 5 and 6 includes the three ChlF parameters, 30 SRIs, or the data fusion of both ChlF parameters and SRIs.

3. Results

3.1. Relationship between leaf chlorophyll fluorescence parameters (ChlF) and grain yield (GY)

The F_v/F_m and Φ_{PSII} showed significant and positive relationships with GY, while the *NPQ* exhibited significant and negative relationship with GY (Fig. 1). The relationship between Φ_{PSII} and GY described by a linear model and the curvilinear relationship were the best models describing the relationships between the other two ChlF (F_v/F_m and NPQ) and GY (Fig. 1). In general, the F_v/F_m showed a moderate relationship with GY (R^2 = 0.64 and 0.60), while the association of GY with Φ_{PSII} (R^2 = 0.80 and 0.83) and *NPQ* (R^2 = 0.82 and 0.86) were high in first and second season, respectively (Fig. 1).

Under individual salinity level, the values of F_v/F_m, Φ_{PSII}, and *NPQ* ranged from 0.82 to 0.88, 0.62 to 0.69, and 0.25 to 0.35 under control treatment; from 0.75 to 0.86, 0.42 to 0.67, and 0.28 to 1.25 under moderate salinity level; and from 0.51 to 0.81, 0.32 to 0.54, and 0.49 to 1.5 under high stress level, respectively (Fig. 1).

3.2. Contour map analysis of the spectral data

To select the best SRIs for estimating the three ChlF parameters and GY, a contour map for each parameter was established using the pooled data of salinity levels, cultivars, and seasons (Fig. 2). The different contour maps were divided into two triangles. One of them was established to calculate the SRIs by dividing the spectral reflectance at a greater wavelength by the spectral reflectance at smaller wavelength, while the other triangle was used to calculate the SRIs by dividing the spectral reflectance at a smaller wavelength by the spectral reflectance at greater wavelength (Fig. 2). In this study, the contour maps were established to present the coefficients of determination (R^2) of combinations of two individual wavelengths ranging from 350 to 2500 nm as a SRI ratio. Based on the high values of R^2, the four measured parameters showed a significant relationship with the SRIs which incorporated VIS/VIS, VIS/NIR, NIR/NIR, SWIR/VIS, and SWIR/NIR wavelengths (Fig. 2). In general, the contour map established for *NPQ* exhibited high values for R^2 followed by GY and Φ_{PSII}, while the contour map conducted for F_v/F_m showed moderate values for R^2 (Fig. 2).

3.3. Relationships between measured parameters and different constructed and published SRIs

The relationships between 30 different SRIs (15 indices constructed in this study based on contour maps and 15 indices selected from literature) and measured parameters were analyzed for each salinity level, cultivar, and season, as well as for all the pooled data. The determination coefficients (R^2) of these relationships are shown in Table 2 for each salinity level, Table 3 for each cultivar, and Table 4 for each season and all pooled data.

All the examined SRIs failed to assess Φ_{PSII} and *NPQ*, while 11 and 12 out of the 30 SRIs exhibited moderate relationships with F_v/F_m (R^2 ranged from 0.34 to 0.54) and GY (R^2 ranged from 0.36 to 0.60), respectively, under control treatment. Under moderate salinity level, the majority of examined SRIs showed moderate relationship with F_v/F_m (R^2 ranged from 0.34 to 0.60) and moderate to strong relationships with the other parameters (R^2 ranged between 0.48 and 0.77 for Φ_{PSII}, 0.57 to 0.91 for *NPQ*, and 0.51 to 0.81 for GY). Under high salinity level, several SRIs showed strong relationships with the four parameters. For example, 17, 12, 20, and 12 out of the 30 SRIs for F_v/F_m, Φ_{PSII}, *NPQ*, and GY, respectively, had R^2 values ≥ 0.70 (Table 2). SRI (R_{690}/R_{630}) and WABI were the only SRIs that failed to estimate the variation in the four measured parameters under moderate salinity level. SRI (R_{1650}/R_{531}) and DWABI-3 also failed to assess the variation in the four measured parameters under high salinity level and F_v/F_m under moderate salinity level. Four other SRIs also failed to estimate the variation in F_v/F_m under moderate salinity levels (i.e., PRI, Cl_{740}, NDRE, and MTCI) (Table 2).

Data in Table 3 show that the majority of SRIs exhibited moderate relationships with the three ChlF (R^2 ranged from 0.23 to 0.65) and moderate to strong relationship with the GY (R^2 ranged from 0.32 to 0.83) for salt-tolerant cultivar Sakha 93, whereas they showed moderate relationships with only F_v/F_m and a strong relationship with the other two parameters of ChlF (Φ_{PSII} and *NPQ*) and GY for salt-sensitive cultivar Sakha 61. Among all examined SRIs, the SRIs (R_{630}/R_{550}), (R_{1950}/R_{750}), (R_{1950}/R_{1050}), (R_{690}/R_{630}), SIPI, DNDMI, and DDMCI failed to estimate the variations in the three ChlF parameters for Sakha 93, whereas only (R_{690}/R_{630}) and WABI failed to estimate variations in the same parameters for Sakha 61. Five out of the 30 SRIs for Sakha 93 (i.e. R_{1950}/R_{750}, R_{1950}/R_{1050}, SIPI, DNDMI, and DDMCI), and only one of the 30 SRIs for Sakha 61 (WABI) failed to estimate GY (Table 3).

For each season and pooled data, all tested SRIs exhibited moderate to strong relationships with four measured parameters (see bold value in Table 4), with the exception of SRI (R_{690}/R_{630}) and WABI, which failed to assess the F_v/F_m and *NPQ* in the first season and the four measured parameters in second season and in all pooled data.

3.4. PLSR models for predicting grain yield

The different models of PLSR based on three ChlF parameters, SRIs, or data fusion of combined SRIs and ChlF parameters were established to predict the GY for each salinity level, cultivar, and season. These models were calibrated using the dataset of pooled data through cross-validation, and subsequently the equations of calibration of different models (Table 5) were used to predict the GY (as independent data) for each salinity level, cultivar, and season (Table 6).

The results showed that the three models of PLSR performed well with regard to predicting GY under all conditions (salinity levels, cultivars, and seasons), with the exception of PLSR model that was based on ChlF parameters, which failed to predict the GY under control treatment (Table 6). The R^2 values for significant PLSR models that were based on the three ChlF parameters, SRIs, or data fusion of combined SRIs and ChlF parameters ranged from 0.80 to 0.95 under moderate salinity level, 0.77 to 0.96 under high salinity level, 0.60 to 0.87 for Sakha 93, 0.92 to 0.98 for Sakha 61, 0.82 to 0.96 for first season, and 0.84 to 0.92 for second season (Table 6). In general,

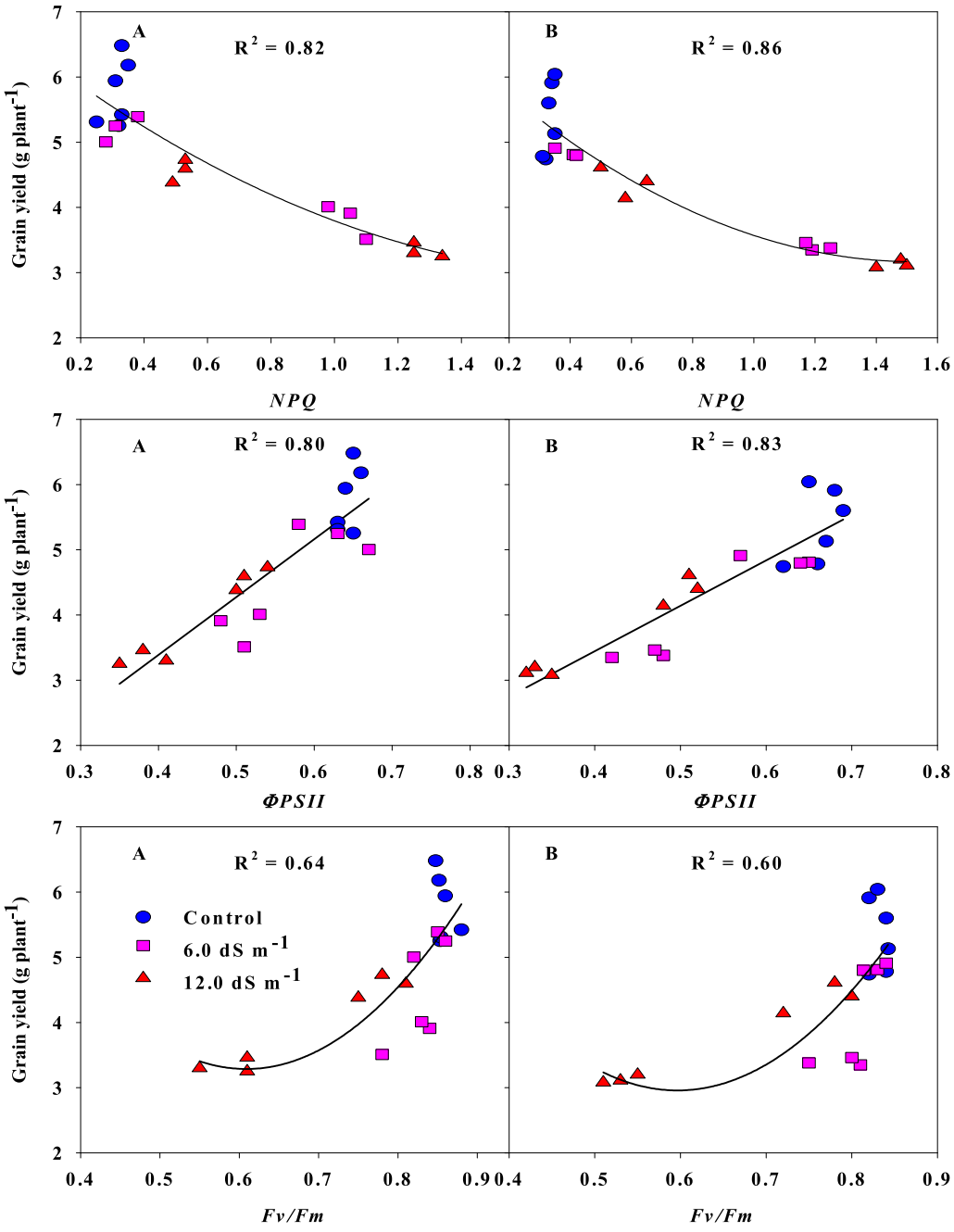

Fig. 1. Relationship between chlorophyll fluorescence parameters (maximum quantum PSII photochemical efficiency (*Fv/Fm*), quantum yield of PSII (Φ_{PSII}), and non-photochemical quenching (NPQ) and grain yield per plant (n = 18) in first (A) and second (B) seasons.

irrespective of conditions, the PLSR model based on data fusion was the best model to predict GY (R^2 ranged from 0.63 to 0.98) followed by PLSR model based on SRIs (R^2 ranged from 0.47 to 0.92) and PLSR model based on ChlF parameters (R^2 ranged from 0.08 to 0.96) (Table 6).

4. Discussion

4.1. Relationship between the measured parameters and their variations under different salt stress levels

The different components of salinity stress (osmotic stress, specific ion toxicity, and deficits in essential ions) interact in different ways to adversely affect the photosynthetic apparatus of leaves, especially photosystem II (PSII) activity (Chen and Murata, 2011; El-Hendawy et al., 2017a; Sancho-Knapik et al., 2018). These harmful effects on PSII are commonly detected and evaluated by measuring several ChlF parameters (Maxwell and Johnson, 2000; Adams and Demmig-Adams, 2004). Interestingly, the different parameters of ChlF can detect noticeable damage in photosynthetic apparatus before the visible symptoms appeared in the leaves (Zarco-Tejada et al., 2003; Zhang et al., 2012; Kalariya et al., 2019); and therefore, it can be used for early detection of salinity induced stress. For instance, the *Fv/Fm* and NPQ have been extensively used as an indicator for early detection of different abiotic stresses (Naumann et al., 2008a; Bauriegel et al., 2011; Ruban and Murchie, 2012; Maimaitiyiming et al., 2017; Sancho-Knapik et al., 2018). When a plant grows under abiotic stress, the photosynthesis efficiency becomes limited and this ultimately leads to an imbalance between the light energy absorbed and that required for carbon fixation. This excess energy can be relaxed by the heat

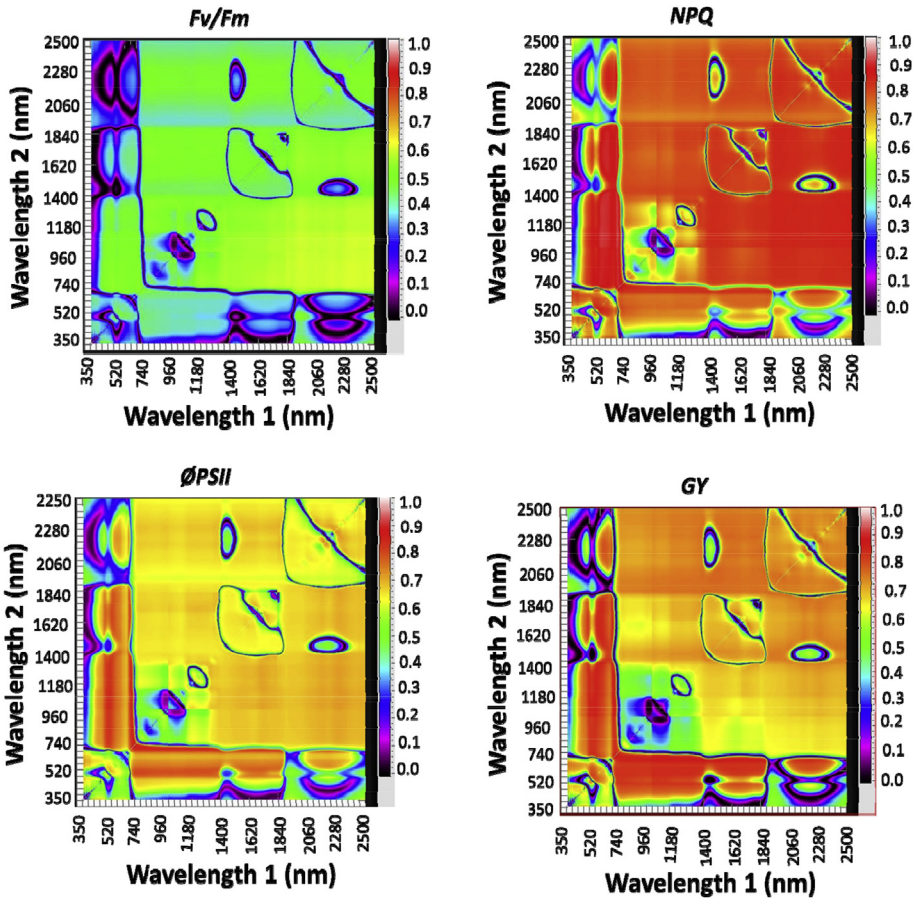

Fig. 2. Contour maps of coefficients of determination (R^2) for all dual wavelength combinations in the spectral range of 350–2500 nm as ratio index. The pooled data of replications, salinity levels, cultivars, and season for maximum quantum PSII photochemical efficiency (*Fv/Fm*), quantum yield of PSII (Φ_{PSII}), non-photochemical quenching (NPQ), and grain yield per plant (GY).

dissipation processes through *NPQ*, which ultimately protect the chloroplast from photodamage (Krause and Weis, 1991; Horton et al., 1996). A decrease in stomatal conductance under salinity stress is often accompanied by a decrease in the Φ_{PSII}, which is used to estimate the photosynthetic linear electron transport (NADPH and ATP) in the thylakoid membranes of the chloroplast (Murchie and Lawson, 2013). Consequently, there is an increasing interest in the use of these parameters of ChlF as screening criteria for evaluating salt tolerance or minimizing irreversible physiological damage induced by salinity stress due to their preliminary and indicative response to rapid changes in plant photosynthetic status. As observed from the results of this study, the final GY significantly decreased with increasing salinity levels, and these decreases were accompanied by a parallel decrease in *Fv/Fm* and Φ_{PSII} and increase in *NPQ* (Fig. 1). In addition, the Φ_{PSII} and *NPQ* were successfully differentiated between the two cultivars even under moderate salinity level. The change in both parameters was more pronounced in salt-sensitive cultivar Sakha 61 than in salt-tolerant cultivar Sakha 93 (Fig. 1). The decrease in Φ_{PSII} exhibited by Sakha 61 may be related to the significant decrease in stomatal conductance. However, the ability of Sakha 93 to maintain stomatal conductance under salt stress could maintain a higher capacity of Φ_{PSII} than did Sakha 61 (El-Hendawy et al., 2017a). The value of *Fv/Fm* was less than the standard value of this parameter for C_3 plants under normal conditions (the standard value of *Fv/Fm* ranged from 0.80 to 0.86), especially for the salt-sensitive cultivar Sakha 61 under high salinity level. In addition, the value of *Fv/Fm* in Sakha 61 under moderate salinity level and the value exhibited by Sakha 93 under moderate and high salinity levels were comparable to the standard value (Fig. 1). The little variations in *Fv/Fm* and the substantial variations in *ΦPSII* and *NPQ* between the two cultivars may explain why the former ChlF parameter exhibited a weaker relationship with GY than the latter two parameters (Fig. 1). The significant associations between GY and these three parameters of ChlF on the one hand, and the ability of these parameters to distinguish salt-tolerance of the two cultivars on the other hand confirm that the incorporation of these ChlF parameters in genetic salinity studies will be critical for improving the chances of identifying wheat cultivars well-adapted to salinity stress, as well as to further improve GY that could derived from improvements of photosynthesis-related traits.

4.2. Performance of spectral reflectance indices (SRIs) for assessment of ChlF parameters

Because the platform of plant growth may influence canopy characteristics, especially under salinity conditions, the spectral reflectance pattern of the canopy will be affected accordingly, which finally affects the efficiency of SRIs for the assessment of ChlF parameters. In our previous studies, we found that different published and modified SRIs have been successful in estimating key physiological traits (e.g., leaf gas exchange, plant water status, ion contents) under simulated saline field conditions using the SWRT-growth platform (El-Hendawy et al., 2019a, b).

The photochemical reflectance index (PRI) is the most important among the SRIs frequently used for tracking the rapid changes in several photosynthetic-related traits under both normal and abiotic stresses at the leaf, canopy, or ecosystem level. This index incorporates the reflectance at 531 nm, which is directly related to the amount of xanthophyll cycle pigments involved in the dissipation of excess energy through *NPQ* and also other carotenoid pigments such as neoxanthin and lutein (Gitelson et al., 2002). Therefore, the reflectance at 531 nm is functionally associated with the de-epoxidation state of xanthophyll cycle pigment, and this association is more obvious under abiotic stresses (Evain et al., 2004; Harris, 2008; Naumann et al., 2008b; Ripullone et al., 2011; Maimaitiyiming et al., 2017; Kováč et al., 2018). Therefore, the PRI index is increasingly used in the studies exploiting

Table 2
Coefficients of determination (R^2) of the relationships between spectral reflectance indices (SRIs) and measured parameters (maximum quantum PSII photochemical efficiency (*Fv/Fm*), quantum yield of PSII (*ΦPSII*), non-photochemical quenching (NPQ), and grain yield per plant (GY) under each salinity level (n = 12).

SRIs	Control				Moderate salinity level				High salinity level			
	Fv/Fm	ΦPSII	NPQ	GY	Fv/Fm	ΦPSII	NPQ	GY	Fv/Fm	ΦPSII	NPQ	GY
R_{570}/R_{870}	0.26	0.04	0.06	0.30	**0.40**	**0.76**	**0.87**	**0.80**	**0.74**	**0.76**	**0.82**	**0.75**
R_{630}/R_{550}	**0.36**	0.17	0.03	0.12	**0.34**	**0.56**	**0.79**	**0.78**	**0.78**	**0.70**	**0.77**	**0.71**
R_{630}/R_{800}	**0.42**	0.00	0.01	0.28	**0.40**	**0.74**	**0.89**	**0.85**	**0.75**	**0.72**	**0.78**	**0.71**
R_{630}/R_{1100}	**0.34**	0.00	0.03	**0.36**	**0.39**	**0.76**	**0.91**	**0.87**	**0.79**	**0.76**	**0.82**	**0.76**
R_{670}/R_{780}	**0.47**	0.01	0.00	0.28	**0.41**	**0.71**	**0.85**	**0.83**	**0.73**	**0.70**	**0.75**	**0.68**
R_{780}/R_{531}	0.20	0.04	0.07	0.30	**0.39**	**0.72**	**0.80**	**0.71**	**0.66**	**0.73**	**0.80**	**0.73**
R_{780}/R_{690}	0.30	0.00	0.02	**0.49**	**0.39**	**0.62**	**0.82**	**0.78**	**0.72**	**0.73**	**0.80**	**0.76**
R_{970}/R_{690}	0.25	0.01	0.02	**0.51**	**0.40**	**0.64**	**0.84**	**0.80**	**0.70**	**0.71**	**0.79**	**0.74**
R_{1100}/R_{670}	0.30	0.01	0.02	**0.40**	**0.38**	**0.58**	**0.79**	**0.77**	**0.73**	**0.75**	**0.82**	**0.76**
R_{1250}/R_{690}	0.23	0.01	0.02	**0.60**	**0.39**	**0.63**	**0.84**	**0.82**	**0.73**	**0.73**	**0.82**	**0.77**
R_{1650}/R_{531}	0.25	0.08	0.03	**0.44**	0.26	**0.61**	**0.60**	**0.51**	0.04	0.10	0.11	0.12
R_{1450}/R_{670}	**0.43**	0.00	0.01	**0.44**	**0.34**	**0.61**	**0.81**	**0.80**	**0.70**	**0.67**	**0.70**	**0.73**
R_{1950}/R_{750}	**0.46**	0.19	0.00	0.08	**0.60**	**0.50**	**0.75**	**0.75**	**0.70**	**0.66**	**0.72**	**0.64**
R_{1950}/R_{1050}	0.33	0.15	0.02	0.16	**0.59**	**0.52**	**0.77**	**0.78**	**0.71**	**0.68**	**0.75**	**0.67**
R_{2250}/R_{670}	**0.53**	0.03	0.04	0.24	**0.35**	**0.56**	**0.78**	**0.77**	**0.82**	**0.76**	**0.81**	**0.80**
NDVI	**0.44**	0.00	0.00	**0.36**	**0.40**	**0.70**	**0.86**	**0.84**	**0.78**	**0.74**	**0.80**	**0.74**
SIPI	0.18	0.02	0.04	0.00	**0.36**	**0.71**	**0.88**	**0.83**	**0.54**	**0.54**	**0.56**	**0.49**
R_{690}/R_{630}	0.32	0.01	0.01	0.08	0.04	0.05	0.09	0.15	**0.46**	**0.41**	**0.50**	**0.46**
PR1	**0.52**	0.09	0.00	0.12	0.26	**0.64**	**0.77**	**0.72**	**0.78**	**0.70**	**0.73**	**0.70**
WAB1	0.19	0.22	0.03	**0.43**	0.00	0.03	0.00	0.00	**0.45**	**0.37**	**0.41**	**0.35**
DWABI-1	**0.54**	0.01	0.03	0.33	**0.34**	**0.55**	**0.57**	**0.59**	**0.35**	**0.39**	**0.46**	**0.43**
DWABI-2	**0.54**	0.01	0.03	0.31	**0.39**	**0.62**	**0.67**	**0.68**	**0.58**	**0.60**	**0.69**	**0.63**
DWABI-3	0.27	0.11	0.02	**0.42**	0.26	**0.64**	**0.61**	**0.54**	0.04	0.09	0.10	0.12
DNDMI	0.03	0.00	0.06	0.12	**0.50**	**0.58**	**0.75**	**0.77**	**0.59**	**0.58**	**0.70**	**0.63**
DDMCI	0.03	0.01	0.11	0.29	**0.51**	**0.48**	**0.66**	**0.68**	**0.55**	**0.59**	**0.71**	**0.63**
CI_{705}	0.04	0.06	0.08	0.31	**0.38**	**0.74**	**0.87**	**0.80**	**0.73**	**0.76**	**0.83**	**0.77**
CI_{740}	0.01	0.04	0.16	0.28	0.24	**0.77**	**0.76**	**0.63**	**0.42**	**0.58**	**0.60**	**0.54**
CI_{green}	0.20	0.04	0.07	0.29	**0.38**	**0.71**	**0.82**	**0.72**	**0.71**	**0.76**	**0.82**	**0.76**
NDRE	0.02	0.04	0.16	0.28	0.24	**0.76**	**0.76**	**0.63**	**0.43**	**0.58**	**0.60**	**0.54**
MTCI	0.02	0.12	0.10	0.13	0.25	**0.59**	**0.62**	**0.53**	**0.45**	**0.60**	**0.63**	**0.58**

The bold values indicate significant relationships at the 0.05 probability level.

simultaneous chlorophyll fluorescence parameters measurements. Our results demonstrated that the ability of PRI for assessing the three ChlF parameters is dependent on salinity levels, cultivars, and seasons (Tables 2–4). The PRI had strong relationships with the three parameters under high salinity level (R^2 = 0.70–0.78), and Φ_{PSII} and NPQ under moderate salinity levels (R^2 = 0.64–0.77); however, it had a moderate relationship with only *Fv/Fm* (R^2 = 0.52) and failed to assess the other two parameters under control treatment condition. In addition, the relationship between PRI and the three ChlF parameters was greater for Sakha 61 than for Sakha 93, as well as for the second season and the pooled data than that for the first season (Tables 3 and 4). Previous studies have reported that PRI index exhibit a good association with ChlF parameters, especially with Φ_{PSII} and NPQ; however, the power of this association is dependent on different plant species, growth stages, and the levels of stress (Gamon et al., 1992; Naumann et al., 2010; Rahimzadeh-Bajgiran et al., 2012; Zhang et al., 2018). The current study indicates that the alternation in many biochemical processes, especially chlorophyll content, due to dynamic responses to the level of salinity stress and mechanisms adaptation, lead to changes in spectral reflectance properties. This may be a main reason to explain why the strength of the relationships between PRI and ChlF parameters are significantly affected by the conditions of measurements in this study (salinity levels, cultivars and, seasons).

Because the functional status of photosynthetic machinery is directly and indirectly sensitive to changes in water and biochemical contents and internal structure of the leaves, which are indirectly influenced by osmotic and ionic stresses of salinity, a number of studies have reported that the SRIs that can track these changes may also prove to be useful for estimating ChlF parameters. Successful examples of such SRIs were found to include structure insensitive pigment index (SIPI), normalized difference vegetation index (NDVI), and water balance index (WABI); the wavelengths incorporated in these indices are able to track the changes in the ratio between carotenoid and chlorophyll *a*, structure of the leaves, photosynthetic function, leaf water content, and *NPQ* for healthy or stressed plants (Harris, 2008; Maimaitiyiming et al., 2017; Rapaport et al., 2017; Miloš et al., 2018; Zhang et al., 2017; Sancho-Knapik et al., 2018). Our results revealed that like PRI, the SIPI, NDVI, DWABI-1, DWABI-2, and DWABI-3 exhibited moderate to strong relationships with ChlF parameters based on conditions (Tables 2–4). In addition, the new SRIs constructed in this study also demonstrated moderate to strong relationships with ChlF parameters, and at times some of them were better than PRI in assessing the ChlF parameters (Tables 2–4). These new SRIs were formulated as reflectance ratios and were based on the combined information from the photosynthetic pigment and fluorescence emission bands found in the visible (VIS, 531, 550, 570, 630, 670, and 690 nm) and red edge (750 and 780 nm) regions, weak absorption bands located in the near-infrared (NIR, 800, 870, 970, 1050, 1100, and 1250 nm) region, and the strong water absorption bands found in the shortwave-infrared (SWIR, 1450, 1650, 1950, and 2250 nm) region. These results indicate that the SRIs that are able to simultaneously monitor two independent mechanisms (i.e., alterations in leaf water status or internal leaf structure and related to alterations in photosynthetic pigments or chlorophyll fluorescence) are also useful for tracking the changes in ChlF parameters under abiotic stresses. Some studies have also reported that the simple spectral reflectance ratio indices such as R_{690}/R_{600}, R_{690}/R_{630}, R_{690}/R_{655}, R_{740}/R_{800} and R_{680}/R_{935} and normalized indices such as WABI and $(R_{680} - R_{935})/(R_{680} + R_{935})$ can be used for spectral assessment of the effect of drought or salinity stresses on different components of ChlF, because the wavelengths used for these indices are very sensitive to co-variation in pigment concentration, red edge reflectance/absorption, superimposition at the red reflectance region, and several key physiological characteristics of leaves (Meroni et al., 2009; Zarco-Tejada et al., 2009; Zhang et al., 2012, 2017; Furuuchi et al.,

Table 3
Coefficients of determination (R^2) of the relationships between spectral reflectance indices (SRIs) and measured parameters (maximum quantum PSII photochemical efficiency (*Fv/Fm*), quantum yield of PSII (*ΦPSII*), non-photochemical quenching (NPQ), and grain yield per plant (GY) for each cultivar (n = 18).

SRIs	Salt-tolerant cultivar (Sakha 93)				Salt-sensitive cultivar (Sakha 61)			
	Fv/Fm	ΦPSII	NPQ	GY	Fv/Fm	ΦPSII	NPQ	GY
R_{570}/R_{870}	0.36	0.60	0.59	0.67	0.46	0.79	0.90	0.87
R_{630}/R_{550}	0.15	0.07	0.05	**0.34**	**0.38**	**0.68**	**0.83**	**0.81**
R_{630}/R_{800}	**0.35**	**0.46**	**0.43**	**0.65**	**0.44**	**0.74**	**0.85**	**0.81**
R_{630}/R_{1100}	**0.36**	**0.48**	**0.46**	**0.69**	**0.42**	**0.76**	**0.88**	**0.85**
R_{670}/R_{780}	**0.23**	**0.26**	**0.23**	**0.51**	**0.44**	**0.70**	**0.80**	**0.76**
R_{780}/R_{531}	**0.38**	**0.54**	**0.51**	**0.74**	**0.42**	**0.80**	**0.90**	**0.91**
R_{780}/R_{690}	**0.36**	**0.44**	**0.40**	**0.76**	**0.39**	**0.76**	**0.91**	**0.92**
R_{970}/R_{690}	**0.34**	**0.44**	**0.41**	**0.77**	**0.38**	**0.76**	**0.91**	**0.92**
R_{1100}/R_{670}	**0.30**	**0.33**	**0.30**	**0.72**	**0.39**	**0.76**	**0.91**	**0.93**
R_{1250}/R_{690}	**0.36**	**0.45**	**0.42**	**0.79**	**0.38**	**0.76**	**0.91**	**0.92**
R_{1650}/R_{531}	**0.40**	**0.58**	**0.60**	**0.75**	**0.30**	**0.70**	**0.81**	**0.87**
R_{1450}/R_{670}	**0.46**	**0.43**	**0.44**	**0.83**	**0.29**	**0.68**	**0.83**	**0.88**
R_{1950}/R_{750}	0.02	0.03	0.02	0.15	**0.59**	**0.68**	**0.75**	**0.69**
R_{1950}/R_{1050}	0.02	0.05	0.04	0.17	**0.60**	**0.72**	**0.80**	**0.74**
R_{2250}/R_{670}	**0.41**	**0.37**	**0.37**	**0.79**	**0.32**	**0.68**	**0.84**	**0.89**
NDVI	**0.23**	**0.27**	**0.25**	**0.52**	**0.43**	**0.73**	**0.85**	**0.82**
SIPI	0.09	0.04	0.01	0.15	**0.37**	**0.53**	**0.58**	**0.51**
R_{690}/R_{630}	0.22	0.18	0.17	**0.32**	0.10	0.22	0.19	**0.28**
PR1	**0.47**	**0.31**	**0.23**	**0.60**	**0.41**	**0.64**	**0.81**	**0.78**
WAB1	**0.40**	**0.56**	**0.62**	**0.58**	0.00	0.06	0.06	0.11
DWABI-1	**0.32**	**0.40**	**0.53**	**0.73**	**0.30**	**0.63**	**0.72**	**0.80**
DWABI-2	**0.29**	**0.39**	**0.51**	**0.71**	**0.35**	**0.68**	**0.78**	**0.84**
DWABI-3	**0.39**	**0.61**	**0.65**	**0.71**	**0.26**	**0.67**	**0.78**	**0.84**
DNDMI	0.05	0.15	0.19	**0.31**	**0.57**	**0.80**	**0.88**	**0.85**
DDMCI	0.05	0.18	0.20	**0.30**	**0.60**	**0.81**	**0.91**	**0.89**
CI_{705}	**0.43**	**0.62**	**0.55**	**0.77**	**0.40**	**0.78**	**0.91**	**0.90**
CI_{740}	**0.34**	**0.68**	**0.61**	**0.66**	**0.42**	**0.79**	**0.85**	**0.80**
CI_{green}	**0.41**	**0.54**	**0.51**	**0.75**	**0.41**	**0.79**	**0.90**	**0.90**
NDRE	**0.34**	**0.68**	**0.61**	**0.65**	**0.42**	**0.79**	**0.85**	**0.80**
MTCI	**0.41**	**0.75**	**0.68**	**0.62**	**0.39**	**0.72**	**0.82**	**0.79**

The bold values indicate significant relationships at the 0.05 probability level.

2013; Ni et al., 2015; Rapaport et al., 2017).

4.3. Comparison of SRIs and partial least squares regression (PLSR) analysis to model grain yield

Although several SRIs have considerable potential for accurately estimating the measured parameters of interest, these SRIs are only based on 2–3 sensitive wavelengths, which makes it difficult to build a unified SRI that can cope with potentially confounding factors relating to measurements and environmental conditions. Therefore, to improve the prediction accuracy of relevant measured parameters, several studies have used the PLSR method that is based on full-spectrum (350–2500 nm) wavelengths, multiple sensitive wavelengths, or multiple SRIs (Hansen et al., 2003; Weber et al., 2012; Li et al., 2014; Sharabian et al., 2014; Elsayed et al., 2017; Feng et al., 2018). For example, Hansen et al. (2003) reported that the PLSR method based on multiple SRIs successfully explained up to 97% of the variation in the grain yield of wheat and barley under different agronomic practices, and Weber et al. (2012) found that the PLSR method explained between 40% and 69% of the variation in the grain yield of maize and also that the prediction models explained more variability in stress conditions than in normal ones. Elsayed et al. (2017) found that using five various SRIs in PLSR analysis increased the accuracy of canopy water content estimations and the grain yield of wheat under normal and water stress conditions. However, Maimaitiyiming et al. (2017) reported that the PLSR method did not improve the estimation of *Gs* and *NPQ* under water stress conditions compared to that of individual SRIs. In addition, Inoue et al. (2016) reported that multivariate models using multiple wavebands proved inferior to a simple model using the ratio spectral index when estimating the canopy chlorophyll content. In this study, several SRIs exhibited strong relationships with GY under all conditions, with the exception of control condition, wherein very few SRIs showed a moderate to weak relationships with GY (Tables 2–4). From these results, we observed that the wavelengths incorporated in these effective SRIs have been found in literature to be very sensitive to variations in chlorophyll pigments, ChlF, photosynthetic efficiency, internal leaf structure, and leaf water status (Lara et al., 2016; Rischbeck et al., 2016; Maimaitiyiming et al., 2017; Silva-Perez et al., 2018; El-Hendawy et al., 2019b).

Interestingly, our results demonstrated that all the PLSR models, based on either the three ChlF parameters, all the examined SRIs, or data fusion of combined ChlF and SRIs exhibited additional improvements for estimating and predicting GY in both the calibration and validation datasets (Tables 5 and 6), when compared to the method using individual SRIs. The PLSR model based on data fusion was the best model to accurately estimate the GY in the validation model under all conditions. This model showed the highest value for the coefficient of determination (R^2) and slope, and the lowest values for root mean square error (RMSE) (Table 6). A similar result was reported by Sharabian et al. (2014); Rischbeck et al. (2016); and Elsayed et al. (2017) for assessing GY of barley and wheat under contrasting water stress conditions; they reported that the PLSR models based on the data fusion of combined SRIs and thermal canopy temperature could improve the quality and robustness of GY predictions compared to individual SRIs or PLSR models that were only based on SRIs. The present study once again confirms that fusing data for combining relevant non-spectral data and spectral bands provides some additional improvements in the accurate estimation of GY of wheat under different conditions. This is because this method can cope with potentially confounding factors relating to measurements and environmental conditions; and therefore, can cover all of the main physiological changes in plants induced by salt-stress.

Table 4
Coefficients of determination (R^2) of the relationships between spectral reflectance indices (SRIs) and measured parameters (maximum quantum PSII photochemical efficiency (*Fv/Fm*), quantum yield of PSII (*ΦPSII*), non-photochemical quenching (NPQ), and grain yield per plant (GY) for each season (n = 18) and pooled data (n = 36).

SRIs	First season				Second season				Pooled data			
	Fv/Fm	ΦPSII	NPQ	GY	Fv/Fm	ΦPSII	NPQ	GY	Fv/Fm	ΦPSII	NPQ	GY
R_{570}/R_{870}	**0.48**	**0.75**	**0.82**	**0.87**	**0.54**	**0.83**	**0.92**	**0.81**	**0.52**	**0.80**	**0.88**	**0.82**
R_{630}/R_{550}	**0.31**	**0.42**	**0.65**	**0.68**	**0.57**	**0.79**	**0.97**	**0.79**	**0.45**	**0.62**	**0.82**	**0.73**
R_{630}/R_{800}	**0.43**	**0.61**	**0.80**	**0.81**	**0.58**	**0.80**	**0.94**	**0.77**	**0.52**	**0.73**	**0.88**	**0.76**
R_{630}/R_{1100}	**0.43**	**0.64**	**0.82**	**0.83**	**0.55**	**0.82**	**0.95**	**0.80**	**0.50**	**0.74**	**0.90**	**0.80**
R_{670}/R_{780}	**0.39**	**0.53**	**0.77**	**0.75**	**0.59**	**0.77**	**0.91**	**0.73**	**0.51**	**0.67**	**0.85**	**0.71**
R_{780}/R_{531}	**0.41**	**0.71**	**0.63**	**0.86**	**0.46**	**0.81**	**0.79**	**0.77**	**0.43**	**0.74**	**0.70**	**0.82**
R_{780}/R_{690}	**0.39**	**0.63**	**0.66**	**0.84**	**0.49**	**0.85**	**0.90**	**0.88**	**0.44**	**0.73**	**0.76**	**0.85**
R_{970}/R_{690}	**0.39**	**0.64**	**0.65**	**0.85**	**0.47**	**0.84**	**0.88**	**0.88**	**0.43**	**0.72**	**0.75**	**0.85**
R_{1100}/R_{670}	**0.37**	**0.60**	**0.62**	**0.84**	**0.49**	**0.84**	**0.91**	**0.86**	**0.42**	**0.68**	**0.73**	**0.84**
R_{1250}/R_{690}	**0.39**	**0.63**	**0.65**	**0.85**	**0.47**	**0.84**	**0.89**	**0.90**	**0.42**	**0.72**	**0.76**	**0.87**
R_{1650}/R_{531}	**0.33**	**0.68**	**0.52**	**0.74**	**0.23**	**0.62**	**0.52**	**0.67**	**0.29**	**0.61**	**0.51**	**0.71**
R_{1450}/R_{670}	**0.37**	**0.63**	**0.65**	**0.81**	**0.37**	**0.76**	**0.78**	**0.88**	**0.37**	**0.65**	**0.68**	**0.83**
R_{1950}/R_{750}	**0.45**	**0.44**	**0.66**	**0.65**	**0.70**	**0.73**	**0.88**	**0.65**	**0.60**	**0.62**	**0.78**	**0.63**
R_{1950}/R_{1050}	**0.46**	**0.47**	**0.68**	**0.68**	**0.70**	**0.76**	**0.91**	**0.69**	**0.60**	**0.64**	**0.81**	**0.66**
R_{2250}/R_{670}	**0.35**	**0.59**	**0.65**	**0.77**	**0.44**	**0.79**	**0.84**	**0.89**	**0.39**	**0.65**	**0.71**	**0.81**
NDVI	**0.39**	**0.55**	**0.78**	**0.78**	**0.58**	**0.79**	**0.94**	**0.78**	**0.50**	**0.70**	**0.87**	**0.76**
SIPI	**0.27**	**0.38**	**0.66**	**0.58**	**0.58**	**0.64**	**0.76**	**0.57**	**0.45**	**0.53**	**0.68**	**0.51**
R_{690}/R_{630}	0.13	**0.31**	0.12	**0.31**	0.05	0.05	0.13	0.12	0.01	0.04	0.00	0.05
PR1	**0.31**	**0.48**	**0.65**	**0.72**	**0.56**	**0.83**	**0.97**	**0.83**	**0.43**	**0.65**	**0.80**	**0.76**
WAB1	0.10	**0.33**	0.12	0.21	0.06	0.00	0.02	0.02	0.00	0.09	0.02	0.11
DWABI-1	**0.42**	**0.67**	**0.65**	**0.81**	**0.26**	**0.62**	**0.62**	**0.66**	**0.34**	**0.61**	**0.62**	**0.74**
DWABI-2	**0.44**	**0.67**	**0.71**	**0.84**	**0.36**	**0.71**	**0.75**	**0.73**	**0.41**	**0.67**	**0.72**	**0.79**
DWABI-3	**0.36**	**0.71**	**0.56**	**0.72**	**0.21**	**0.61**	**0.55**	**0.68**	**0.28**	**0.64**	**0.55**	**0.70**
DNDMI	**0.55**	**0.58**	**0.63**	**0.75**	**0.52**	**0.76**	**0.93**	**0.77**	**0.53**	**0.69**	**0.80**	**0.74**
DDMCI	**0.55**	**0.60**	**0.65**	**0.80**	**0.51**	**0.74**	**0.89**	**0.72**	**0.52**	**0.68**	**0.79**	**0.74**
CI_{705}	**0.42**	**0.71**	**0.69**	**0.87**	**0.49**	**0.86**	**0.86**	**0.85**	**0.45**	**0.78**	**0.78**	**0.85**
CI_{740}	**0.41**	**0.76**	**0.62**	**0.80**	**0.44**	**0.81**	**0.79**	**0.78**	**0.42**	**0.78**	**0.70**	**0.77**
CI_{green}	**0.40**	**0.70**	**0.63**	**0.86**	**0.46**	**0.82**	**0.80**	**0.78**	**0.43**	**0.74**	**0.71**	**0.82**
NDRE	**0.42**	**0.77**	**0.63**	**0.80**	**0.45**	**0.81**	**0.80**	**0.79**	**0.43**	**0.78**	**0.71**	**0.78**
MTCI	**0.41**	**0.70**	**0.58**	**0.71**	**0.40**	**0.79**	**0.72**	**0.77**	**0.40**	**0.74**	**0.64**	**0.72**

The bold values indicate significant relationships at the 0.05 probability level.

Table 5
Equations and the Coefficients of determination (R^2) of partial least squares regression (PLSR) models based on chlorophyll fluorescence parameters (ChlF), all examined spectral reflectance indices (SRIs), and data fusion of combined ChlF and SRIs that were used to predict the grain yield per plant presented in Table 6.

Models	Calibration equations of PLSR	R^2
Model ChlF	y = 0.8235x + 0.8081	**0.82*****
Model SRIs	y = 0.8565x + 0.6568	**0.86*****
Data fusion	y = 0.9409x + 0.2705	**0.94*****

*, **, *** indicate significance at 0.05, 0.01 and 0.001 P level, respectively.

5. Conclusion

The results of this study indicated that it was possible to assess ChlF parameters, which their measurements with traditional method remain laborious and time-consuming as well such measurements are not feasible when they are made on a large scale (about two measurements per hour), using specific individual SRIs, but the strengths of the relationships between ChlF parameters and SRIs depended on salinity levels and cultivars. Some selected indices that are simultaneously based on water absorption bands, chlorophyll bands, and red edge bands were much more effective for estimating ChlF than PRI, which is being functionally associated with the de-epoxidation state of xanthophyll cycle pigment. The PLSR models based on data fusion of SRIs and ChlF parameters provide additional improvements for estimating GY even under control conditions when compared with individual SRIs.

The results from the current study are important since the relationships between the measured parameters and spectral reflectance indices, as well as the different models of partial least squares regression for predicting grain yield were tested under different salinity levels (control, moderate, and high level) and for two cultivars differing in salt tolerance. Therefore, when we need to apply the results of this study under natural saline field conditions, we should first classify the salinity levels of soil (moderate or high salinity level) and the variation in spatial heterogeneity in soil salinity should be very limited for each salinity level, which is absolutely necessary for the homogeneous growth of wheat plants. To overcome the high variation in the spatial heterogeneity in natural saline field conditions, which is not suitable for growing wheat, one would have to apply agronomic management practices such as mixing large quantities of gypsum into the soil and using effective drainage schemes and leaching portions in order to obtain a uniform plant growth for a wheat population and application of hyperspectral reflectance method for high-throughput assessment of photosynthetic status and prediction of wheat production under salt stress field conditions with either moderate or high salinity levels.

Author Contributions

SE-H and SE performed the experiments and edited the manuscript, SE-H, NA, MA, and WH designed the experiment and followed upon data collection, SE-H, SE, NA, MA, SE and US analysed the data, SE-H, NA, and WH Canopy spectral reflectance measurements, SE-H and US Final approval of the version to be published

Acknowledgments

The authors extend their appreciation to the Deanship of Scientific Research at King Saud University, Saudi Arabia for funding this work through Research Group No. (RG-1435-032) and the Researchers Support & Services Unit (RSSU) for their technical support.

Table 6
Prediction models, equations, root mean square error (RMSE), and coefficient of determination (R^2) of the different models of partial least squares regression (PLSR) based on chlorophyll fluorescence parameters (ChlF), all examined spectral reflectance indices (SRIs), or data fusion (combined ChlF and SRIs). These models were calibrated using the dataset of pooled data through cross-validation, and subsequently the equations of calibration of different models (Table 5) were used to predict the GY (as independent data) for each salinity level, cultivar, and season.

Treatments	Prediction Models	Equations	RMSE (g/plant)	R^2
Control	Model ChlF	y = −0.0254x + 5.4589	0.60	0.08
	Model SRIs	y = 0.4084x + 3.346	0.39	**0.47***
	Data fusion	y = 0.5074x + 2.7662	0.33	**0.63****
Moderate salinity level (6.0 dS m^{-1})	Model ChlF	y = 1.0097x + 0.115	0.23	**0.95*****
	Model SRIs	y = 0.7941x + 0.7345	0.39	**0.80*****
	Data fusion	y = 0.947x + 0.1745	0.18	**0.95*****
High salinity level (6.0 dS m^{-1})	Model ChlF	y = 1.3287x – 1.1761	0.29	**0.96*****
	Model SRIs	y = 0.6518x + 1.4424	0.34	**0.77*****
	Data fusion	y = 0.9609x + 0.1799	0.16	**0.95*****
Sakha 93	Model ChlF	y = 0.2703x + 3.7131	0.52	**0.60****
	Model SRIs	y = 0.833x + 0.6516	0.39	**0.77*****
	Data fusion	y = 0.8049x + 0.9164	0.27	**0.87*****
Sakha 61	Model ChlF	y = 1.1167x – 0.401	0.24	**0.95*****
	Model SRIs	y = 1.087x – 0.1337	0.34	**0.92*****
	Data fusion	y = 1.1286x – 0.4185	0.20	**0.98*****
First season	Model ChlF	y = 0.751x + 1.1049	0.42	**0.82*****
	Model SRIs	y = 0.9085x + 0.3472	0.39	**0.85*****
	Data fusion	y = 0.9575x + 0.1852	0.19	**0.96*****
Second season	Model ChlF	y = 0.9199x + 0.4295	0.39	**0.84*****
	Model SRIs	y = 0.8238x + 0.8647	0.34	**0.88*****
	Data fusion	y = 0.9253x + 0.3461	0.27	**0.92*****

*, **, *** indicate significance at 0.05, 0.01 and 0.001 P level, respectively.

References

Kováč, D., Veselovská, P., Klem, K., Věcěrová, K., Ač, A., Peñuelas, J., Urban, O., 2018. Potential of photochemical reflectance index for indicating photochemistry and light use efficiency in leaves of European beech and Norway spruce trees. Remote Sens. 10, 1202. https://doi.org/10.3390/rs10081202.

Abdeshahian, M., Nabipour, M., Meskarbashee, M., 2010. Chlorophyll fluorescence as criterion for the diagnosis salt stress in wheat (*Triticum aestivum*) plants. Proc. World Acad. Sci. Eng. Technol. 71, 569–571.

Adams III, W.W., Demmig-Adams, B., 2004. Chlorophyll fluorescence as a tool to monitor plant response to the environment. In: In: Papageorgiou, G.C., Govindjee (Eds.), Advances in Photosynthesis and Respiration, vol. 19. Springer, Berlin, pp. 583–604.

Ahmed, I.M., Cao, F., Zhang, M., Chen, X., Zhang, G., Wu, F., 2013. Difference in yield and physiological features in response to drought and salinity combined stress during anthesis in Tibetan wild and cultivated barleys. PLoS One 8 (10), e77869. https://doi.org/10.1371/journal.pone.0077869.

Asner, G.P., Alencar, A., 2010. Drought impacts on the Amazon forest: the remote sensing Perspective. New Phytol. 187, 569–578.

Atzberger, C., Guérif, M., Baret, F., Werner, W., 2010. Comparative analysis of three chemometric techniques for the spectroradiometric assessment of canopy chlorophyll content in winter wheat. Comput. Electron. Agric. 73, 165–173.

Babar, M.A., Reynolds, M.P., van Ginkel, M., Klatt, A.R., Raun, W.R., Stone, M.L., 2006. Spectral reflectance indices as a potential indirect selection criteria for wheat yield under irrigation. Crop Sci. 46, 578–588. https://doi.org/10.2135/cropsci2005.0059.

Baker, N.R., 2008. Chlorophyll fluorescence: a probe of photosynthesis in vivo. Annu. Rev. Plant Biol. 59, 89–113.

Baker, N.R., Rosenqvist, E., 2004. Applications of chlorophyll fluorescence can improve crop production strategies: an examination of future possibilities. J. Exp. Bot. 55 (403), 1607–1621.

Bauriegel, E., Giebel, A., Geyer, M., Schmidt, U., Herppich, W.B., 2011. Early detection of Fusarium infection in wheat using hyper-spectral imaging. Comput. Electron. Agric. 75, 304–312.

Bazihizina, N., Barrett-Lennard, E.G., Colmer, T.D., 2012. Plant growth and physiology under heterogeneous salinity. Plant Soil 354, 1–19.

Buschmann, C., Langsdorf, G., Lichtenthaler, H.K., 2000. Imaging of the blue, green, and red fluorescence emission of plants: an overview. Photosynthetica (Prague) 38 (4), 483–491.

Cetin, M., Kirda, C., 2003. Spatial and temporal changes of soil salinity in a cotton field irrigated with low-quality water. J. Hydrol. 272, 238–249.

Chen, T.H., Murata, N., 2011. Glycinebetaine protects plants against abiotic stress: mechanisms and biotechnological applications. Plant Cell Environ. 34, 1–20.

Çullu, M.A., AydemIR, S., Qadir, M., Almaca, A., Öztürkmen, A.R., Biligç, A., Agca, N., 2009. Implication of groundwater fluctuation on the seasonal salt dynamic in the Harran Plain, south-eastern Turkey. Irrig. Drain. 59, 465–476.

Dash, J., Curran, J., 2004. The MERIS terrestrial chlorophyll index. Int. J. Remote Sens. 25, 5403–5413.

Dobrowski, S.Z., Pushnik, J.C., Zarco-Tejada, P.J., Ustin, S.L., 2005. Simple reflectance indices track heat and water stress-induced changes in steady-state chlorophyll fluorescence at the canopy scale. Remote Sens. Environ. 97, 403–414.

El-Hendawy, S.E., Hassan, W.M., Al-Suhaibani, N.A., Refay, Y., Abdella, K.A., 2017a. Comparative performance of multivariable agro-physiological parameters for detecting salt tolerance of wheat cultivars under simulated saline field growing conditions. Front. Plant Sci. 8, 435. https://doi.org/10.3389/fpls.2017.00435.

El-Hendawy, S.E., Hassan, W.M., Refay, Y., Schmidhalter, U., 2017b. On the use of spectral reflectance indices to assess agro-morphological traits of wheat plants grown under simulated saline field conditions. J. Agron. Crop Sci. 203, 406–428. https://doi.org/10.1111/jac.12205.

El-Hendawy, S.E., Al-Suhaibani, N., Hassan, W., Dewir, Y.H., El-Sayed, S., Al-Ashkar, I., Abdella, K.A., Schmidhalter, U., 2019a. Evaluation of wavelengths and spectral reflectance indices for high throughput assessment of growth, water relations and ion contents of wheat irrigated with saline water. Agric. Water Manag. 212, 358–377.

El-Hendawy, S.E., Al-Suhaibani, N., Dewir, Y.H., El-Sayed, S., Alotaibi, M., Hassan, W.M., Refay, Y., Tahir, M.U., 2019b. Ability of modified spectral reflectance indices for estimating growth and photosynthetic efficiency of wheat under saline field conditions. Agronomy 9, 35. https://doi.org/10.3390/agronomy9010035.

Elsayed, S., Elhewity, M., Ibrahim, H.H., Dewir, Y.H., Migdadi, H.M., Schmidhalter, U., 2017. Thermal imaging and passive reflectance sensing to estimate the water status and grain yield of wheat under different irrigation regimes. Agric. Water Manag. 189, 98–110.

Evain, S., Flexas, J., Moya, I., 2004. A new instrument for passive remote sensing: 2. Measurement of leaf and canopy reflectance changes at 531 nm and their relationship with photosynthesis and chlorophyll fluorescence. Remote Sens. Environ. 91, 175–185.

Feng, M., Guo, X., Wang, C., Yang, W., Shi, C., Ding, G., Zhang, X., Xiao, L., Zhang, M., Song, X., 2018. Monitoring and evaluation in freeze stress of winter wheat (*Triticum aestivum* L.) through canopy hyperspectrum reflectance and multiple statistical analysis. Ecol. Indicat. 84, 290–297.

Filella, I., Peñuelas, J., Llorens, L., Estiarte, M., 2004. Reflectance assessment of seasonal and annual changes in biomass and CO_2 uptake of a Mediterranean shrubland submitted to experimental warming and drought. Remote Sens. Environ. 90, 308–318.

Furuuchi, H., Jenkins, M.W., Senock, R.S., Houpis, J.L.J., Pushnik, J.C., 2013. Estimating plant crown transpiration and water use efficiency by vegetative reflectance indices associated with chlorophyll fluorescence. Open J. Ecol. 3, 122–132.

Gamon, J., Peñuelas, J., Field, C.A., 1992. narrow-waveband spectral index that tracks diurnal changes in photosynthetic efficiency. Remote Sens. Environ. 41, 35–44.

Garriga, M., Romero-Bravo, S., Estrada, F., Escobar, A., Matus, I.A., del Pozo, A., Astudillo, C.A., Lobos, G.A., 2017. Assessing wheat traits by spectral reflectance: do we really need to focus on predicted trait-values or directly identify the elite

genotypes group? Front. Plant Sci. 8, 280. https://doi.org/10.3389/fpls.2017.00280.
Gitelson, A.A., Merzlyak, M.N., 1997. Remote estimation of chlorophyll content in higher plant leaves. Int. J. Remote Sens. 18, 2691–2697.
Gitelson, A.A., Buschmann, C., Lichtenthaler, H.K., 1998. Leaf chlorophyll fluorescence corrected for re-absorption by means of absorption and reflectance measurements. J. Plant Physiol. 152, 283–296.
Gitelson, A.A., Zur, Y., Chivkunova, O.B., Merzlyak, M.N., 2002. Assessing carotenoid content in plant leaves with reflectance spectroscopy. Photochem. Photobiol. 75, 272–281.
Gitelson, A., Gritz, Y., Merzlyak, M., 2003. Relationships between leaf chlorophyll content and spectral reflectance and algorithms for non-destructive chlorophyll assessment in higher plant leaves. J. Plant Physiol. 160, 271–282. https://doi.org/10.1078/0176-1617-00887.
Gitelson, A.A., Vina, A., Rundquist, D.C., Ciganda, V., Arkebauer, T.J., 2005. Remote estimation of canopy chlorophyll content in crops. Geophys. Res. Lett. 32, 93–114 108403 10.1029/2005Gl022688.
Hansen, P.M., Jorgensen, J.R., Thomsen, A., 2003. Predicting grain yield and protein content in winter wheat and spring barley using repeated canopy reflectance measurements and partial least squares regression. J. Agric. Sci. Camb. 139, 307–318.
Harris, A., 2008. Spectral reflectance and photosynthetic properties of Sphagnum mosses exposed to progressive drought. Ecohydrology 1, 35–42.
Horton, P., Ruban, A.V., Walters, R.G., 1996. Regulation of light harvesting in green plants. Annu. Rev. Plant Physiol. Plant Mol. Biol. 47, 655–684.
Inoue, Y., Guérif, M., Baret, F., Skidmore, A., Gitelson, A., Schlerf, M., Darvishzadeh, R., Olioso, A., 2016. Simple and robust methods for remote sensing of canopy chlorophyll content: a comparative analysis of hyperspectral data for different types of vegetation. Plant Cell Environ. 39, 2609–2623.
Jia, M., Zhou, C., Cheng, T., Tian, Y., Zhu, Y., Cao, W., Yao, X., 2016. Inversion of chlorophyll fluorescence parameters on vegetation indices at leaf scale. In: IEEE International Geoscience and Remote Sensing Symposium (IGARSS), Beijing, China, pp. 4359–4362. https://doi.org/10.1109/IGARSS.2016.7730136.
Jin, S., Wang, P., Zhao, K., Yang, Y., Yao, S., Jiang, D., 2004. Characteristics of gas exchange and chlorophyll fluorescence in different position leaves at booting stage in rice plants. Rice Sci. 11 (5–6), 283–289.
Kalariya, K.A., Goswami, N., Mehta, D., Singh, A.L., Saran, P.L., 2019. Chlorophyll Fluorescence: a physiological mechanism and a physical tool in plant eco-physiological studies. In: In: Hemantaranjan, A. (Ed.), Advances in Plant Physiology, vol. 18. Scientific Publishers Inc., pp. 201–242.
Krause, G., Weis, E., 1991. Chlorophyll fluorescence and photosynthesis: the basics. Annu. Rev. Plant Physiol. Plant Mol. Biol. 42, 313–349.
Lara, M.A., Diezma, B., Lléo, L., Roger, J.M., Garrido, Y., Gil, M.I., Ruiz-Altisent, M., 2016. Hyperspectral imaging to evaluate the effect of irrigation water salinity in lettuce. Appl. Sci. 6 (12), 412. https://doi.org/10.3390/app6120412.
Li, F., Mistele, B., Hu, Y., Chen, X., Schmidhalter, U., 2014. Reflectance estimation of canopy nitrogen content in winter wheat using optimised hyperspectral spectral indices and partial least squares regression. Eur. J. Agron. 52, 198–209. https://doi.org/10.1016/j.eja.2013.09.006.
Lichtenthaler, H.K., Miehé, J.A., 1997. Fluorescence imaging as a diagnostic tool for plant stress. Trends Plant Sci. 2, 316–320.
Maimaitiyiming, M., Ghulam, A., Bozzolo, A., Wilkins, J.L., Kwasniewski, M.T., 2017. Early detection of plant physiological responses to different levels of water stress using reflectance spectroscopy. Remote Sens. 9, 745. https://doi.org/10.3390/rs9070745.
Mariotto, I., Thenkabail, P.S., Huete, A., Slonecker, E.T., Platonov, A., 2013. Hyperspectral versus multispectral crop-productivity modeling and type discrimination for the HyspIRI mission. Remote Sens. Environ. 139, 291–305.
Maxwell, K., Johnson, G.N., 2000. Chlorophyll fluorescence—a practical guide. J. Exp. Bot. 51, 659–668.
Meroni, M., Rossini, M., Guanter, L., Alonso, L., Rascher, U., Colombo, R., 2009. Remote sensing of solar-induced chlorophyll fluorescence: review of methods and applications. Remote Sens. Environ. 113, 2037–2051.
Miloš, B., Josef, H., Jana, M., Kateřina, S., Alica, K., 2018. Dehydration-induced changes in spectral reflectance indices and chlorophyll fluorescence of Antarctic lichens with different thallus color, and intrathalline photobiont. Acta Physiol. Plant. 40, 177. https://doi.org/10.1007/s11738-018-2751-3.
Murchie, E.H., Lawson, T., 2013. Chlorophyll fluorescence analysis: a guide to good practice and understanding some new applications. J. Exp. Bot. 64, 3983–3998. https://doi.org/10.1093/jxb/ert208.
Najafi, F., Khavari-Nejad, R.A., Rastgar-Jazii, F., Sticklen, M., 2007. Growth and some physiological attributes of pea (*Pisum sativum* L.) as affected by salinity. Pak. J. Biol. Sci. 10, 2752–2755. https://doi.org/10.3923/pjbs.2007.2752.2755.
Naumann, J.C., Youngm, D.R., Anderson, J.E., 2008a. Leaf chlorophyll fluorescence, reflectance, and physiological response to freshwater and saltwater flooding in the evergreen shrub, *Myrica cerifera*. Environ. Exp. Bot. 63, 402–409. https://doi.org/10.1016/j.envexpbot.2007.12.008.
Naumann, J.C., Anderson, J.E., Young, D.R., 2008b. Linking physiological responses, chlorophyll fluorescence and hyperspectral imagery to detect salinity stress using the physiological reflectance index in the coastal shrub, Myrica cerifera. Remote Sens. Environ. 112, 3865–3875.
Naumann, J.C., Bissett, S.N., Young, D.R., Edwards, J., Anderson, J.E., 2010. Diurnal patterns of photosynthesis, chlorophyll fluorescence, and PRI to evaluate water stress in the invasive species, Elaeagnus umbellata Thunb. Trees 24, 237–245.
Ni, Z.Y., Liu, Z.G., Huo, H.Y., Li, Z.L., Nerry, F., Wang, Q.S., Li, X.W., 2015. Early water stress detection using leaf-level measurements of chlorophyll fluorescence and temperature data. Remote Sens. 7, 3232–3249.
Peng, Y., Zeng, A., Zhu, T., Fang, S., Gong, Y., Tao, Y., Zhou, Y., Liu, K., 2017. Using remotely sensed spectral reflectance to indicate leaf photosynthetic efficiency derived from active fluorescence measurements. J. Appl. Remote Sens. 11 (2), 026034. https://doi.org/10.1117/1.JRS.11.026034.
Peñuelas, J., Baret, F., Filella, I., 1995. Semi-empirical indices to assess carotenoids/chlorophyll a ratio from leaf spectral reflectance. Photosynthetica 31, 221–230.
Porcar-Castell, A., Tyystjärvi, E., Atherton, J., van der Tol, C., Flexas, J., Pfündel, E.E., Moreno, J., Frankenberg, C., Berry, J.A., 2014. Linking chlorophyll a fluorescence to photosynthesis for remote sensing applications: mechanisms and challenges. J. Exp. Bot. 65, 4065–4095.
Rahimzadeh-Bajgiran, P., Munehiro, M., Omasa, K., 2012. Relationships between the photochemical reflectance index (PRI) and chlorophyll fluorescence parameters and plant pigment indices at different leaf growth stages. Photosynth. Res. 113, 261–271.
Rapaport, T., Hochberg, U., Cochavi, A., Karnieli, A., Rachmilevitch, S., 2017. The potential of the spectral 'water balance index' (WABI) for crop irrigation scheduling. New Phytol. 216, 741–757. https://doi.org/10.1111/nph.14718.
Ripullone, F., Rivelli, A.R., Baraldi, R., Guarini, R., Guerrieri, R., Magnani, F., Peñuelas, J., Raddi, S., Borghetti, M., 2011. Effectiveness of the photochemical reflectance index to track photosynthetic activity over a range of forest tree species and plant water statuses. Funct. Plant Biol. 38, 177–186.
Rischbeck, P., Elsayed, S., Mistele, B., Barmeier, G., Heil, K., Schmidhalter, U., 2016. Data fusion of spectral, thermal and canopy height parameters for improved yield prediction of drought stressed spring barley. Eur. J. Agron. 78, 44–59. https://doi.org/10.1016/j.eja.2016.04.013.
Ruban, A.V., Murchie, E.H., 2012. Assessing the photoprotective effectiveness of non-photochemical chlorophyll fluorescence quenching: a new approach. Biochim. Biophys. Acta 1817, 977–982.
Sancho-Knapik, D., Mendoza-Herrer, Ó., Gil-Pelegrín, E., Peguero-Pina, J.J., 2018. Chl fluorescence parameters and leaf reflectance indices allow monitoring changes in the physiological status of *Quercus ilex* L. under progressive water deficit. Forests 9, 400. https://doi.org/10.3390/f9070400.
Sharabian, V.R., Noguchi, N., Ishi, K., 2014. Significant wavelengths for prediction of winter wheat growth status and grain yield using multivariate analysis. Eng. Agric. Environ. Food 7 (1), 14–21.
Silva-Perez, V., Molero, G., Serbin, S.P., Condon, A.G., Reynolds, M.P., Furbank, R.T., Evans, J.R., 2018. Hyperspectral reflectance as a tool to measure biochemical and physiological traits in wheat. J. Exp. Bot. 69 (3), 483–496.
Tucker, C.J., 1979. Red and photographic infrared linear combinations for monitoring vegetation. Remote Sens. Environ. 8, 127–150.
Weber, V.S., Araus, J.L., Cairns, J.E., Sanchez, C., Melchinger, A.E., Orsini, E., 2012. Prediction of grain yield using reflectance spectra of canopy and leaves in maize plants grown under different water regimes. Field Crop. Res. 128, 82–90. https://doi.org/10.1016/j.fcr.2011.12.016.
Zarco-Tejada, P.J., Pushnik, J.C., Dobrowski, S.Z., Ustin, S.L., 2003. Steady state chlorophyll a fluorescence detection from canopy derivative reflectance and double-peak red-edge effects. Remote Sens. Environ. 84, 283–294. https://doi.org/10.1016/S0034-4257(02)00113-X.
Zarco-Tejada, P.J., Berni, J.A.J., Suárez, L., Sepulcre-Cantó, G., Morales, F., Miller, J.R., 2009. Imaging chlorophyll fluorescence with an airborne narrow-band multispectral camera for vegetation stress detection. Remote Sens. Environ. 113, 1262–1275.
Zhang, H., Zhua, L., Hu, H., Zhen, K., Jina, Q., 2011. Monitoring leaf chlorophyll fluorescence with spectral reflectance in rice (*Oryza sativa* L.). Procedia Eng. 15, 4403–4408.
Zhang, H., Hu, H., Zhang, X., Wang, K., Song, T., Zeng, F., 2012. Detecting *Suaeda salsa* L. chlorophyll fluorescence response to salinity stress by using hyperspectral reflectance. Acta Physiol. Plant. 34, 581–588. https://doi.org/10.1007/s11738-011-0857-y.
Zhang, L., Ma, H., Chen, T., Pen, J., Yu, S., 2014. Morphological and physiological responses of cotton (*Gossypium hirsutum* L.) plants to salinity. PLoS One 9, e112807. https://doi.org/10.1371/journal.pone.0112807.
Zhang, C., Preece, C., Filella, I., Farré-Armengol, G., Peñuelas, J., 2017. Assessment of the response of photosynthetic activity of mediterranean evergreen oaks to enhanced drought stress and recovery by using PRI and R690/R630. Forests 8 (10). https://doi.org/10.3390/f8100386.
Zhang, Y.J., Hou, M.Y., Xue, H.Y., Liu, L.T., Sun, H.C., Li, C.D., Dong, X.J., 2018. Photochemical reflectance index and solar-induced fluorescence for assessing cotton photosynthesis under water-deficit stress. Biol. Plant. 62 (4), 817–825.